Research Square

Preprints are preliminary reports that have not undergone peer review.
They should not be considered conclusive, used to inform clinical practice,
or referenced by the media as validated information.

Multi-Omics analysis to identify the metabolic mechanism of the ethanol extract of Gymnadenia Conopsea R.Br. in hyperuricemia treatment

Tianrong CHEN

189899191050163.com

Xizang Academy of Agricultural and Animal Husbandry Sciences

Jiale LIU

Xizang Academy of Agricultural and Animal Husbandry Sciences

Chengling NIE

Xizang Academy of Agricultural and Animal Husbandry Sciences

Siyuan YANG

Xizang Academy of Agricultural and Animal Husbandry Sciences

Fuchen JIA

Xizang Academy of Agricultural and Animal Husbandry Sciences

Yuhong ZHANG

Xizang Academy of Agricultural and Animal Husbandry Sciences

Article

Keywords: Gymnadenia Conopsea R.Br., hyperuricemia, zebrafish, metabolomics, transcriptomics

Posted Date: December 16th, 2024

DOI: https://doi.org/10.21203/rs.3.rs-5076138/v1

License: This work is licensed under a Creative Commons Attribution 4.0 International License.
Read Full License

Additional Declarations: No competing interests reported.

Abstract

Background: The ethanol extract of *Gymnadenia Conopsea R.Br.* (Gym) has been shown to significantly lower uric acid levels. However, its uric acid reducing mechanism has not been studied from a multi-omics perspective.

Objective: By conducting multiple omics studies and analyzing the metabolic characteristics of the ethanol extract of Gym on zebrafish with hyperuricemia (HUA), we aimed to provide insights into its metabolic mechanism during HUA treatment.

Methods: Non-targeted metabolomics studies were conducted using ultra-high performance liquid chromatography-Q-Exactive mass spectrometry (UHPLC-QE MS). Samples were sequenced using second-generation sequencing technology on the Illumina sequencing platform, to perform paired-end sequencing of the gene library.

Results: Different concentrations and doses of ethanol extracts of Gym significantly reversed the levels of 33 common biomarkers, including sphingosine, plant sphingosine, unsaturated fatty acids, and amino acids. These biomarkers were mainly involved in phenylalanine, tyrosine, and tryptophan biosynthesis, phenylalanine metabolism, ABC transporter activity, PPAR signaling pathway, linoleic acid metabolism, and unsaturated fatty acid biosynthesis.

Conclusion: The ethanol extract of Gym can exhibit therapeutic effects on HUA by participating in amino acid biosynthesis pathways, amino acid metabolism, linoleic acid metabolism, ABC transport, and unsaturated fatty acid biosynthesis. This result provides a reference for elucidating the metabolic mechanism of Gym for the treatment of HUA.

1. Introduction

Hyperuricemia (HUA) refers to the condition in which the fasting serum uric acid (SUA) level is higher than 420 μmol/L in males and 360 μmol/L in females on two different days under a regular purine diet (Han et al., 2017; Zhang et al., 2019). In China, approximately 120 million patients have high uric acid levels, accounting for about 10% of the total population. This condition has become the second-largest metabolic disease after diabetes (Wu et al., 2017). Although considerable progress has been made in the study of HUA pathogenesis in recent years, lifestyle changes over the past few decades; high purine, high sugar, high fat diets; frequent late nights, irregular work and rest patterns, lack of exercise, age, and genetic factors have all contributed to an increase in the incidence rate of HUA. Notably, there is a trend of HUA affecting young individuals (Jin et al., 2012). Therefore, it is necessary to develop rapid, accurate, and reliable treatment methods to assess individuals with these conditions.

Drugs commonly used for treating HUA include allopurinol (APL), febuxostat, and benzbromarone, but these drugs are associated with certain side effects (Sapankaew et al., 2022; Li et al., 2023). In recent years, the continuous development of traditional Chinese medicine has enabled the increased use of

edible Chinese medicinal materials or herbal for the treatment of various diseases, including HUA and gout. ChondroT is a new type of Chinese herbal medicine composed of water extracts obtained from plants such as osterici radix, lonicerae folium, angelicae gigantis radix, clematidis radix, and phellodendri cortex. Dool Ri Oh et al. (2019) have shown that ChondroT can improve HUA by regulating xanthine oxidase (XOD) activity and renal mURAT1. A study performed by Wu Hui et al. (2016)has shown that emodinol extracted from the rhizomes of *Elaeagus pungens* can lower SUA levels in mice, inhibit liver XOD activity, promote the expression of UA excretion-related proteins, and exhibit UA-lowering and renal protective effects. It can potentially be used as a drug for treating HUA and renal dysfunction. A study by Ferid Abdulhafiz et al. (2020) has shown that ethanolic extracts of *Alocasia longiloba* fruits and petioles have strong DPPH and ABTS scavenging activities, and can significantly inhibit XOD activity. Thus, these extracts could serve as a new medicinal material for treating HUA. HUA is associated with imbalances in some metabolites. Some studies have reported metabolic differences between HUA patients, healthy individuals, and gout patients, and found that metabolic pathways associated with amino acid, lipid, carbohydrate, and energy metabolism were disrupted in HUA and gout patients (Zhang et al., 2018; Wu et al., 2023). However, few multi-omics methods can be used to explore the therapeutic mechanisms by which these Chinese medicinal herbs or extracts affect HUA.

Gymnadenia conopsea R.Br. (Gym) is a traditional medicinal plant that contains various functional components, such as flavonoids, polysaccharides, polyphenols, alkaloids, and terpenes, as well as nutrients, such as proteins, amino acids, minerals, and crude fibers. It can tonify the kidney, nourish essence, promote blood circulation, remove blood stasis, regulate qi, and relieve pain (Cai et al., 2006; Shang et al., 2017; Wang et al., 2020). Modern pharmacological studies have shown that the ethanol extract derived from Gym has significant effects on clearing free radicals, enhancing the immune response, reducing fatigue, improving memory, reducing creatinine and uric acid levels, and alleviating the symptoms of HUA (Zeng et al., 2007; Zhang et al., 2013; Lin et al., 2021). However, there is hardly any research on the mechanism by which this drug facilitates the prevention and treatment of HUA from the metabolomics perspective. Therefore, studying the regulatory and therapeutic mechanisms of the ethanol extract of Gym on endogenous metabolism through transcriptomic and metabolomic analysis is of great significance for the clinical treatment of HUA.

An acute HUA zebrafish model was constructed in this study using potassium oxazinate (PO) and xanthine sodium salt (XSS). Metabolomics and transcriptomics analysis were performed using UHPLC-QE MS and second-generation sequencing technology. Principal component analysis (PCA), partial least squares discriminant analysis (PLS-DA), and orthogonal partial least squares discriminant analysis (OPLS-DA) were used to detect changes in metabolite profiles in zebrafish samples. The study explores the molecular mechanisms and related metabolic pathways of the ethanol extract of Gym for the treatment of HUA, providing a basis its clinical application and the development of related health products.

2. Materials and Methods

2.1 Plant materials

Gym was obtained from the market (Xizang, Lhasa, China), washed with distilled water, dried in an oven at 40℃ to remove surface moisture, crushed with a universal grinder, passed through a 60-mesh sieve, and dried to a constant weight in an oven at 40℃.

2.2 Extraction of ethanol extract from Gym

The extraction of uric acid lowering substances from Gym was performed using the XOD inhibition rate as the indicator. The key factors considered were the ethanol concentration, solid-liquid ratio, ultrasound power, extraction time, and extraction temperature. During the experiment, it was found that the 95% ethanol extract of Gym had a significantly stronger XOD inhibition rate compared to the 75% ethanol extract. The extraction rate of the 75% ethanol extract of Gym was much higher than that of the 95% ethanol extract. Considering factors such as cost and extraction volume, ethanol concentrations of 95% and 75% were selected for experiment optimization. The optimal extraction process was achieved under the conditions of a 1:40 solid-liquid ratio, 500 W ultrasound power at 70℃, and ultrasound-assisted extraction for 80 minutes. Under these conditions, the extraction rates of the 95% and 75% ethanol extracts of Gym were approximately 4.0% and 14.0%, respectively. Related optimization processes and material comparisons can be found in previously published reports (Chen et al., 2022).

2.3 Construction of an acute HUA zebrafish model

A zebrafish model of HUA was established based on the model proposed by ZHANG Yingyu et al. (2019). We selected 1080 wild-type juvenile AB zebrafish with normal development and randomly divided them into 6 groups (control, model, and APL group, Treatment A: 500 mg/L 95% Gym ethanol extract, Treatment B: 250 mg/L 95% Gym ethanol extract, Treatment C: 500 mg/L 75% Gym ethanol extract. Effective concentrations were selected based on previous reports (Chen et al., 2022)). Each group had with 3 compound wells that were placed in a 6-well plate (n = 20 per group), and 3 parallel experiments were conducted. Each well had a volume of 4 mL, and each culture dish was labeled with details showing the group and treatment status. All groups except for the control group were first treated with PO and XSS at 28℃, and pre-incubated for 1 hour, after which corresponding doses of APL were added and aqueous Gym solutions were extracted. All treatment groups were cultured in a constant temperature incubator at 28℃ for 24 hours to perform metabolite and RNA sample extraction. Euthanasia and Collection of Zebrafish Juvenile by Incubation with Tricaine Solution. This experiment has been approved by the Center for Mitochondrial Health and Aging Research conducted by Yantai University (China).

2.4 Non-targeted metabolomics testing

2.4.1 Sample metabolite extraction

First, 60 juvenile zebrafish were randomly selected from each group and placed in a 2 mL centrifuge tube, and 1000 μL of tissue extraction solution (75% (9:1 methanol: chloroform): 25% H_2O) was added,

along with steel balls. Then, these materials were added into a tissue grinder, ground at 50 Hz for 60 seconds, and the above process was repeated twice. Next, the solution was sonicated at room temperature for 30 minutes and placed on ice for 30 minutes, followed by centrifugation at 12000 rpm and 4 ℃ for 10 minutes. The supernatant was added into a centrifuge tube, concentrated, and dried. Finally, 200 μL of prepared 50% acetonitrile solution containing 2-chloro-L-phenylalanine (4 ppm) was used to dissolve the sample. The filtrate was added to the detection bottle for LC-MS detection (Warren et al., 2017).

2.4.2 LC-MS chromatographic conditions

The Thermo Vanquish (Thermo Fisher Scientific, USA) ultra-high performance liquid phase system was used along with an ACQUITY UPLC ® HSS T3 (2.1 × 100 mm, 1.8 μm) (Waters, Milford, MA, USA) chromatography column. The system was operated at a flow rate of 0.3 mL/min, column temperature of 40℃, and injection volume of 2 μL. Positive ion mode; mobile phase consisting of 0.1% formic acid acetonitrile (B1) and 0.1% formic acid water (A1), gradient elution program: 0–1 min, 8% B1; 1–8 minutes, 8%-98% B1; 8–10 minutes, 98% B1; 10-10.1 minutes, 98%-8% B1; 10.1–12 minutes, 8% B1. Negative ion mode; mobile phase consisting of acetonitrile (B2) and 5 mM ammonium formate water (A2), gradient elution program: 0–1 min, 8% B2; 1–8 minutes, 8%-98% B2; 8–10 minutes, 98% B2; 10-10.1 minutes, 98%-8% B2; 10.1–12 minutes, 8% B2 (Zelena, et al., 2009).

2.4.3 LC-MS mass spectrometry conditions

Thermo Orbitrap Exploris 120 mass spectrometer (Thermo Fisher Scientific, USA), electric spray ion source and positive and negative ion modes were used to collect data. The positive ion spray voltage was 3.50 kV, negative ion spray voltage was − 2.50 kV, and 40 arb sheath gas and 10 arb auxiliary gas were used. The capillary temperature was 325℃, and a first-level full scan was performed with a resolution of 60000. The first-level ion scan range was m/z 100–1000, and HCD was used for second-level fragmentation with a collision energy of 30% and a second-level resolution of 15000. The first four ions in the collected signal were fragmented, and unnecessary MS/MS information was removed using dynamic exclusion (Want et al., 2013).

2.4.4 Mass spectrometry peak preprocessing

The raw data was converted to the mzXML file format using the MSConvert tool in the Proteowizard software package (v3.0.8789) (Rasmussen et al., 2022). A quantitative list of metabolites was obtained using the R XCMS (v3.12.0) for peak detection, peak filtering, and peak alignment processing (Navarro-Reig et al., 2015). Key parameter settings include bw = 2, ppm = 15, peakwidth = c(5,30), mzwidth = 0.015, mzdiff = 0.01, and method="centWave". Support vector regression correction based on QC samples was used to eliminate systematic errors. Then, substances with a coefficient of variation (CV) less than 30% were retained in the QC sample for subsequent analysis (Want et al., 2013).

Metabolites were identified using accuracy mass and MS/MS data that were matched with data from the HMDB (http://www.hmdb.ca) (Wishart et al., 2022), massbank (http://www.massbank.jp/) (Horai et al.,

2010), KEGG (https://www.genome.jp/kegg/) (Manish et al., 2007), LipidMaps (http://www.lipidmaps.org) (Abdelrazig et al., 2020), mzcloud(https://www.mzcloud.org) (Kanehisa M and Goto S, 2000), and metabolite databases built by Panomix Biomedical Tech Co., Ltd. (Shuzhou, China). The parameters were set to < 30 ppm, and qualitative results of metabolites were obtained.

2.5 Transcriptome sequencing and gene expression analysis

2.5.1 Sample RNA extraction

Total RNA was extracted from juvenile zebrafish tissues using the TRIzol method (Ujibe et al., 2021). Sixty zebrafish samples were randomly selected from each group and placed in a 2 mL grinding tube and a grinder was used at 60 Hz for 60 seconds. Then, 2–4 samples were taken each time, and 1 mL of TRIzol reagent was added to the ground powder and mixed immediately (the sample needed to be stored at a low temperature until TRIzol was added). After adding all samples to TRIzol, wet beating was performed at 55Hz for 30 seconds and samples were incubated at room temperature for 5 minutes to facilitate the complete separation of nucleosomes in the homogenate sample. Then, the solution was centrifuged at 12000 rpm for 5 minutes, the supernatant was extracted, and RNA was extracted from juvenile zebrafish tissues using TRIzol method. The concentration and purity of RNA were detected using a nanodrop system (Thermo Scientific NanoDrop 2000), and the integrity was detected using RNA-specific agarose electrophoresis and a 2100 detection system (Agilent 2100 Bioanalyzer RNA 6000 Nano kit 5067 − 1511).

2.5.2 Library construction and quality inspection

RNA sequencing (RNA seq) and gene expression analysis were conducted by BioNovoGene (Suzhou, China). A total quantity ≥ 1 μg of total RNA was selected, and the NEBNext Ultra II RNA Library Prep Kit for the Illumina assay kit was used for the preparation of the cDNA library. The Agilent 2100 Bioanalyzer and Agilent High Sensitivity DNA Kit (Agilent, 5067 − 4626) were used for quality testing of the library. Pico Green was used to detect the total concentration of the library (Quantifluor-ST fluorometer, Promega, E6090; Quant it PicoGreen dsDNA Assay Kit, Invitrogen, P7589), and QPCR was used to quantitatively detect the effective library concentration (Thermo Scientific StepOnePlus Real Time PCR Systems). Homogenization of multiple DNA libraries was performed, followed by equal volume mixing. The mixed library was gradually diluted and quantified, and perform PE150 mode sequencing was performed on an Illumina sequencer. An index of the reference genome was built using HISAT2 v2.0.5 and paired-end clean reads were aligned with the reference genome. HTSeq (0.9.1) was used to compare the read count values on each gene with the original expression level of the gene. FPKM (fragments per kilo bases per million fragments) was used to standardize expression levels, and DESeq software (1.20.0) was used for differential expression analysis between two comparative combinations (Zang et al., 2019). The differential analysis of gene expression was performed using DESeq, and the screening conditions for differentially expressed genes were as follows: expression difference multiple | log2FoldChange |>1, significance P < 0.05. TopGO was used for GO enrichment analysis, and the P-value

(significantly enriched standard is P < 0.05) was calculated using the hypergeometric distribution method. GO terms were identified along with significantly enriched differentially expressed genes, and the main biological functions performed by differentially expressed genes were identified. KEGG pathway enrichment analysis was performed using ClusterProfiler (3.4.4) software, with a focus on significantly enriched pathways with a P-value < 0.05 (Yu et al., 2018).

2.6 Combined metabolomics and transcriptomics analysis

Transcriptome sequencing can yield a large number of differentially expressed genes and numerous regulatory networks. Metabolites are the ultimate embodiment of life activities, and small changes in phenotypic traits are exponentially amplified at the metabolic level. The combined analysis of the transcriptome and metabolome allows for the changes in phenotype status to be reflected and enables the genetic mechanisms that affect the phenotype to be explained. Furthermore, it enables mutual verification between two levels of data (Gao et al., 2014).

First, the metabolome and transcriptome data were evaluated to select samples that met the requirements. Then, based on the list of detected differentially expressed substances, they were sorted in the ascending order based on their P-values. By default, the top 50 differentially expressed metabolites and mRNAs were selected for omics correlation analysis.

3. Data statistics and analysis

The data were analyzed using the BioDeep Platform (https://www.biodeep.cn). One-way ANOVA and the Duncan's test ($p < 0.05$) were used to determine significant differences.

4. Results

4.1 Multivariate statistical analysis

In order to systematically elucidate the mechanism of the improvement of HUA using the ethanol extract derived from Gym, we analyzed all zebrafish samples in positive and negative ion modes using UHPLC-QE MS. The base peak chromatograms and total ion chromatograms are shown in Supplementary Figures 1, 2. The PCA score chart and RSD distribution chart of samples are shown in Figure 1 (A, B), with an RSD value of 86.8%. The experimental results indicate that the sample quality, experimental method, and system stability were adequate, showing the reliability of the test results. The performance of PLS-DA and OPLS-DA was good in this study, showing differences between the groups (Figure 1C, E). The permutation test results show that the model was robust, without overfitting, and the model parameters were excellent (R2=(0.0,0.97), Q2=(0.0,0.35), R2=(0.0,0.97), Q2=(0.0,0)), with good predictive ability and interpretability (Figure 1D, F).

4.2 Differential metabolite analysis

Next, we identified metabolites based on MS/MS results and information from online databases, and selected ion characteristics with $p < 0.05$ and VIP > 1.0 as differential metabolites. As a result, a total of 31791 metabolites were screened in the positive ion mode, of which 8121 were differential metabolites; 23964 metabolites were screened in the negative ion mode, of which 5860 were differential metabolites. The metabolites containing secondary spectra in the quantitative list were compared to those with fragmented ions and other information regarding each secondary spectrum in the database, to achieve the secondary qualitative identification of modern metabolites. A total of 359 secondary metabolites were detected this time, of which 94 were differential metabolites (see Supplementary Table 1). The results of the statistical comparison of different metabolites among different groups are shown in Figure 2A. Next, we used hierarchical clustering to analyze differential metabolites in each group (Figure 2B). Compared with the control group, a total of 85 differential metabolites were observed in the model group. These included 3'-AMP, 4-(glutamylamino) butanoate, 5-aminopentanoic acid, 7-methyladenine, 25 hydroxycholesterol, alpha-ketoisovaleric acid, choline, guanidinosuccinic acid, homo L-arginine, inosine, L-homophenylalanine, N-acetylaspartylglutamate, N-acetylornithine, norethindrone, palmitoleic acid, palmitoylethanolamide, prostaglandin A2, D-mannose, and 41 other significantly upregulated differential metabolites. Compared with the model group, the levels of 6, 11, 12, and 9 metabolites were downregulated with APL and Treatment A, Treatment B, and Treatment C groups, respectively (Annex 1 Supplementary Table 2-6). Compared with the control group, levels of (S)-2-methylmalate, 2,3-butanediol, citric acid, deoxycholic acid, deoxyuridine, EPA (d5), epsilon-(gamma-L-glutamyl)-L-lysine, gamma-glutamylcysteine, isoxanthopterin, L-arginine, L-aspartic acid, L-dopa, linoleic acid, L-kynurenine, methyl jasmonate, methyleugenol, myriocin, nicotinamide ribotide, phytosphingosine, prostaglandin I2, sphingosine, and other 44 differential metabolites were significantly downregulated in the model group. However, the levels of 16, 15, 16, and 21 metabolites were significantly increased with APL, treatment A, treatment B, and treatment C groups, respectively, compared to the model group (Annex 1 Supplementary Table 2-6).

Interestingly, we found that the ethanol extract of Gym exhibited a certain consistency with APL in regulating metabolites in HUA. They could significantly upregulate metabolites such as (S) -2-methylmalate, L-dopa, sphingosine, 11,12-DiHETrE, porphybilinogen, alpha-zearalenol, alpha-dimorphecolic acid, gamma-aminobutyric acid, hecogenin, and other metabolites. They could downregulate metabolites such as 3-indoleacrylate, sinapine, N-acetylornithine, anabasine, and indole. Besides, APL had significant effects on the levels of guanidinosuccinic acid, probenecid, 9,10-epoxyoctadecenoic acid, 4,5-dihydroorotic acid, L-tyrosine, N-alpha-acetyllysine, N6-acetyl-L-lysine, and glycylleucine, and could significantly reduce the levels of metabolites such as creatine, creatinine, fumaric acid, and indole. The ethanol extract groups obtained with different concentrations and doses of Gym also showed certain differences. Treatment A had adequate regulatory effects on choline, L-cystine, (2R,3R)-3-methylglutamyl-5-semialdehyde-N6-lysine, guanosine, D-4'-phosphopantothenate, pregnanediol, 2-hydroxy-6-pentadecylbenzoic acid, sodium deoxycholate, 3-dehydroecdysone, probenecid, fumaric acid, o-phosphoethanolamine, gentisic acid, 9,10-epoxyoctadecenoic acid, and prostaglandin F3a levels. Treatment B mainly regulated 8,9-DiHETrE, 2-hydroxycinnamic acid, L-tyrosine,

3-hydroxy-5-methyl-L-tyrosine, ubiquinone-1, 3-dehydrosphinganine, pergolide, 14,15-DiHETrE, prostaglandin E1, tetracosanoic acid, phenyl acetate, thymidine, and cytidine levels. Treatment C mainly regulated beta-alanyl-L-lysine, cortisone, L-alanyl-gamma-D-glutamyl-L-lysine, L-norvaline, and all-trans-retinoic acid levels. Figure 2C shows the changes in differential metabolites among these groups. The results of correlation analysis of these differential metabolites are shown in Figure 2D. In summary, different concentrations and doses of ethanol extracts of Gym significantly reversed the levels of 33 common biomarkers, including sphingosine, phytosphingosine, nicotinamide ribotide, porphobilinogen, L-dopa, L-homophenylalanine, N-acetylornithine, 3-indoleacrylate, and choline.

4.3 Analysis of differential metabolic pathways

KEGG pathway enrichment analysis of the list of differential metabolites was performed using MetaboAnalyst (www.metaboanalysis. ca) (Xia et al., 2011). The enrichment method is based on the hypergeometric distribution test, while the topological analysis adopts the degree of centrality. The results are presented interactively and visually in Figures 3-5.

Compared with the control group, different concentrations and doses of ethanol extracts of Gym mainly participate in arachidonic acid metabolism, alanine, aspartate, and glutamate metabolism, oxidative phosphorylation, mTOR signaling pathway, linoleic acid metabolism, and β-alanine metabolism (Figure 3A, C, E). The main metabolites involved include linoleic acid, 5(S)-HepETE, L-arginine, L-aspartic acid, succinic acid, N-acetyl-L-aspartic acid, N-acetylaspartylglutamate, fumaric acid, PC (18_3(6Z,9Z,12Z)_18_3(6Z-9Z-12Z)), 8,9-DiHETrE, L-glutamine, citric acid, L-aspartate, prostaglandin H2, prostaglandin I2, prostaglandin A2, pantothenic acid, and gamma-aminobutyric acid. (Figures 3B, D, F). These differential pathways and metabolites may be involved in the treatment of HUA. Compared with the control group, the main metabolic pathways involved with APL include those associated with alanine, aspartate, and glutamate metabolism, oxidative phosphorylation, linoleic acid metabolism, arachidonic acid metabolism, arginine biosynthesis, mTOR signaling, and β-alanine metabolism. (Figure 3G). The main metabolites include succinic acid, L-aspartic acid, L-glutamine, L-arginine, fumaric acid, citric acid, gamma-aminobutyric acid, PC (183(6Z,9Z,12Z)_183(6Z,9Z,12Z)), arachidonic acid, linoleic acid, 11,12-diHETrE, and prostaglandin I2, prostaglandin A2, and others (Figure 3H). It can be inferred that there are significant similarities in metabolic pathways and metabolites between the ethanol extracts of Gym and the APL group.

Compared with the control group, potassium oxazinate and sodium xanthine mainly participate in metabolic pathways as associated with linoleic acid metabolism, alanine, aspartate, and glutamate metabolism, PPAR signaling, arginine biosynthesis, and unsaturated fatty acid biosynthesis (Figure 4A). Compared with the model group, the metabolic pathways influenced by different concentrations and doses of ethanol extracts of Gym and APL-positive drugs include those associated with PPAR signaling, arginine biosynthesis, arachidonic acid metabolism, linoleic acid metabolism, alanine, aspartate, and glutamate metabolism, and ABC transport (Figure 4B, C, D, E). The metabolites involved include linoleic acid, 13-L-hydroperoxylinoleic acid, gamma-linolenic acid, 9-OxoODE, alpha-dimorphocolic acid, succinic

acid, L-aspartic acid, citric acid, gamma-aminobutyric acid, prostaglandin H2, prostaglandin I2, 20-carboxy-leukotriene B4, prostaglandin A2, 15-deoxy-d-12, 8,9-DiHETrE, sphinganine, phytosphingosine, and all-trans-retinoic acid. (Figure 5). This could facilitate the research and application of ethanol extracts of Gym in combination therapy. Besides, the characteristic metabolic pathways involved in Gym include those associated with mTOR signaling, D-arginine and D-ornithine metabolism, steroid hormone biosynthesis, sulfur metabolism, pentose and glucuronate interconversions, primary bile acid biosynthesis, purine metabolism, and propionate metabolism. (Supplementary Table 7-10). These differential pathways may lead to different therapeutic effects.

The main metabolic pathways involved in the processing of differential metabolites with ethanol extracts of Gym at different concentrations include those associated with alanine, aspartate, and glutamate metabolism, PPAR signaling pathway, tyrosine metabolism, arginine biosynthesis, ABC transporters, retinol metabolism, linoleic acid metabolism, D-glutamine and D-glutamate metabolism, and oxidative phosphorylation (Supplementary Figures 3A). Metabolites involved include succinic acid, L-glutamine, L-arginine, L-cysteine, fumaric acid, gamma-aminobutyric acid, alpha-dimorphocolic acid, L-dopa, hydroquinone, gentisic acid, 4-hydroxycinnamic acid, sucrose, choline, D-mannose, xanthosine, retinal, 9-cis-retinal, 9-cis-retinal acid, PC(183(6Z,9Z,12Z)_183(6Z,9Z,12Z)), 13-L-hydroperoxylinoleic acid, and pyrrolidonecarboxylic acid (Supplementary Figure 3B). The differences in effective ingredients may lead to different therapeutic effects. It can be further inferred that Gym is an effective ingredient in the treatment of HUA.

In summary, the treatment of PO-induced HUA in zebrafish mainly involves the PPAR signaling pathway, arginine biosynthesis, arachidonic acid metabolism, linoleic acid metabolism, alanine, aspartic and glutamic acid metabolism, ABC transport, oxidative phosphorylation, beta-alanine metabolism, phenylalanine, tyrosine and tryptophan biosynthesis, phenylalanine metabolism, tyrosine metabolism, and retinol metabolism. These results are consistent with those of Huang (2019), Tan (2021), Shan (2021), and others . Moreover, the preliminary research results of this project also indicate that the ethanol extract of Gym mainly participates in metabolic pathways such as those associated with aminoacyl-tRNA biosynthesis, phenylalanine, tyrosine and tryptophan biosynthesis, and phenylalanine metabolism (Chen et al., 2022).

4.4 Analysis of differentially expressed genes

Metabolomics analysis can reflect changes in phenotypic status. However, individual metabolomic testing cannot explain the genetic mechanisms that affect phenotype. Therefore, to further investigate the mechanism of action of the ethanol extract of Gym in HUA zebrafish, we identified the gene expression profiles of zebrafish that were treated or not treated with ethanol extract of Gym using a transcriptomics approach. Transcriptomics is the study of transcriptional information present in biological samples from a holistic perspective. This technology can facilitate the study of the changes in expression levels of genes in different organisms, measure gene expression levels in organisms under different conditions, and thus help to understand diseases and deeply explore the process of disease-

related changes (Marguerat S and Bähler J, 2010). RNA sequencing technology (RNA seq), one of the most popular transcriptomics techniques, uses high-throughput sequencing to capture all sequences. An analysis of the association between metabolomics and transcriptome can overcome the limitations of the aforementioned single omics studies to some extent. By combining transcriptomics techniques to study changes in the organism at the gene level, we can more systematically reveal metabolic data and regulatory mechanisms (Sun and Hu, 2016; Gusev et al., 2016).

The results of screening RNA seq samples are shown in Supplementary Table 11. It can be seen that the values of Q20 (%) and Q30 (%) are both greater than the theoretical value by 90%, indicating good data output quality. In PCA, the control, model, APL, and different concentrations of ethanol extract of the Gym group were significantly separated (Figure 6A). Next, we used DESequence to perform a differential gene expression analysis, with expression difference multiples | log2FoldChange |>1 and significance P-value<0.05 as the screening criteria for differentially expressed genes. The results are represented by volcano plots and bar charts (Figure 6B, C1-C5), and the unique number of differentially expressed genes among the compared groups is shown in Figure 6D. Compared with the control group, a total of 811 differentially expressed genes were screened in the model group, of which 546 were downregulated and 265 were upregulated. Compared with the model group, a total of 1251 differentially expressed genes were screened in the Treatment A group, of which 747 were downregulated and 504 were upregulated. Compared with the model group, a total of 1339 differentially expressed genes were screened in the Treatment B group, of which 561 were downregulated and 778 were upregulated. Compared with the model group, a total of 2710 differentially expressed genes were screened in the Treatment C group, of which 1151 were downregulated and 1559 were upregulated.

4.5 GO functional enrichment analysis of differentially expressed genes

GO enrichment analysis was performed using topGO, and differential genes annotated in GO terms were used to calculate the gene list and number of genes for each term. P<0.05 indicates significant differences (Alexa and Rahnenführer, 2009). The GO enrichment analysis results of differentially expressed genes were classified according to molecular function, biological process, and cellular component. The top 10 most significantly enriched GO term entries in each GO classification process were selected, as shown in Supplementary Figure 4.

As shown in Supplementary Figure 4, differentially expressed genes between the model and control groups were significantly enriched in pathways such as those involved in the regulation of biological quality, calcium ion binding, cytoskeletal protein binding, cytoskeleton, and actin binding. The differential genes between the APL and model groups were significantly enriched in pathways such as those involved in the extracellular region, calcium ion binding, structural molecular activity, and lipid binding. The differential genes between the Treatment A and model groups are mainly enriched in pathways such as those involving the membrane, integral membrane component, and intrinsic membrane component. The differential genes between the Treatment B and model groups are mainly enriched in pathways involving the cytoskeleton, transporter activity, and metal ion binding. The differential genes between the

Treatment C and model groups were mainly enriched in developmental processes, anatomical structure development, system development, multicellular organism development, multicellular organic processes, metal ion binding, cation binding, and other pathways. GO analysis intuitively reflects the distribution of differentially expressed genes in terms of cellular composition, molecular function, and biological processes among different compared groups.

4.6 Analysis of KEGG pathway enrichment of differentially expressed genes

To systematically understand the related functions and pathways of genes, KEGG pathway enrichment analysis can identify the main metabolic and signal transduction pathways involved in the differential expression of genes (Chen et al., 2015). The top 20 enriched signaling pathways are shown in Figure 7. The control and model groups were mainly enriched in histidine metabolism, VEGF, MAPK, and calcium signaling, thiamine metabolism, one-carbon pool by folate, linoleic acid metabolism, alpha-linolenic acid metabolism, and ether lipid metabolism (Figure 7A). The pathways with the most significant enrichment of differentially expressed genes in the ethanol extracts of different concentrations and doses of Gym included ABC transporters, histidine metabolism, phenylalanine metabolism, phenylalanine, tyrosine, and tryptophan biosynthesis, drug metabolism-cytochrome P450, purine metabolism, and linoleic acid metabolism. Besides, these pathways also participated in glycolysis/glycogenesis, metabolism of xenobiotics by cytochrome P450, pentose phosphate pathway, drug metabolism with other enzymes, steroid biosynthesis, retinol metabolism, tyrosine metabolism, and the PPAR signaling pathway.(Figure 7C-E). These metabolic pathways are roughly the same as ALP regulated pathways (Figure 7B). It is hypothesized that treatment with the ethanol extract of Gym can affect the metabolism of zebrafish with HUA to a certain extent. Besides, studies have shown that polysaccharides from goji berries, astragalus membranaceus, and active oligopeptides from sea cucumbers can also improve HUA by affecting related pathways, such as those associated with glycerophospholipid metabolism, tyrosine metabolism, purine metabolism, and linoleic acid metabolism (Hui et al., 2018; Huang et al., 2019; Zhou et al., 2024). The results of this study are consistent with those of aforementioned studies.

4.7 Analysis of the correlation between transcriptomics and metabolomics

Because of the overlap of multiple metabolic pathways between metabolomics and transcriptomics in metabolic pathway analysis, we further conducted correlation analysis between the two omics datasets. In order to identify the key metabolic pathways, metabolites, and genes regulating key metabolites in the treatment of HUA with Gym, we ranked the differentially expressed mRNA and metabolites with $|R| > 0.8$ and $P < 0.05$. By default, the top 50 differentially expressed metabolites and mRNA were selected for Pearson correlation calculation, and graphs were conducted.

It was found that the model group and the control group did not share any common metabolic pathways for differentially expressed genes and metabolites (Figure 8A). The main metabolic pathways involved in differential metabolite generation were those associated with alanine, aspartate, and glutamate metabolism, arginine biosynthesis, PPAR signaling, biosynthesis of unsaturated fatty acids, and linoleic acid metabolism. The main metabolic pathways involved in differential gene expression included those

associated with C-type lectin receptor signaling, MAPK signaling, apoptosis, histidine metabolism, and VEGF signaling. Among these, 13 differentially expressed genes, including *gata3*, *reep2*, *fgfr1a*, *brinp3b*, *tnpo1*, *shisa6*, and *crigm2d1* were significantly positively correlated with 23 differentially expressed metabolites, including N-acetylornithine, norepinephrine, 3-epiecdysone, palmitoylethanolamide, 20-carboxy-leukotriene B4, and 7-methyladenine. There was a significant negative correlation between 27 differential metabolites, including isoxanthopterin, andrographolide gamma-glutamylcysteine, 11,12-diHETrE, thymine, 4-quinolinecarboxylic acid, and methyleugenol. Thirty-seven differentially expressed genes, including Si: ch211-93f2.1, gpr158a, ace2, cdh17, mt-nd4l, actn3a, atp2a1, apobb.1, tnnt3a, apoa2, and ppl were significantly negatively and positively correlated with these 23 and 27 differentially expressed metabolites, respectively (Figure 8B). The network diagrams of some key metabolites and their regulatory genes are shown in Figure 8C.

The metabolic pathways involved in the differential expression of metabolites and genes between the APL group and the model group include those associated with linoleic acid metabolism and PPRA signaling (Supplementary Figure 5A). The main metabolites and genes involved include linoleic acid, 9,10-epoxyoctadecenoic acid, alpha-dimorphocolic acid, 9-cis-retinoic acid, and *apoa1a*, *pck1*, *pck2*, *cd36*, *cyp3a65*, and *si:ch211-214p16.3*. (Supplementary Figure 5B). The correlation heatmap and network diagram are shown in Supplementary Figure 5C-D. Twenty-four differentially expressed genes, including *rcvrn2*, *gnb3b*, *crygm2d10*, *crygm2d7*, *gnat1*, and *prph2b* were significantly positively correlated with 37 differentially expressed metabolites, including gamma-aminobutyric acid, probenecid, L-aspartic acid, N-alpha-acetyllysine, linoleic acid, 9-cis-retinoic acid, 9,10-epoxyoctadecenoic acid, (S)-2-methylmalic acid, and guanidinosuccinic acid. A significant negative correlation was observed with 13 different metabolites, including 3-indomethacrylate, N-acetylornithine, fumaric acid, creatinine, and 8,9-DiHETrE. Twenty-six differentially expressed genes, including *slc13a2*, *apoa4b.1*, *cyp3a65*, *slc15a1b*, *krt4*, and *mt-nd2* were negatively and positively correlated to a significant with these 37 and 13 differentially expressed metabolites, respectively.

The metabolic pathways involved in the differential expression of metabolites and genes in the Treatment A and model groups include those associated with ABC transport, PPRA signaling, and linoleic acid metabolism (Figure 8D). The main metabolites involved include L-glutamine, L-arginine, L-cystine, choline, L-aspartic, xanthosine, linoleic acid, arachidonic acid, and 9-cis-retinoic acid. The genes involved include *abcg2a*, *abcb11a*, *abca2*, *abcc2*, *abcc4*, *abca5*, *apoa1a*, *plin2*, *acsl5*, *cyp3a65*, and *si:ch211-214p16.3*. (Figure 8E). Among these, 17 genes, including egr4, ier2a, sema5d, gnb3b, and nfil3-5, were significantly positively correlated with the expression of 27 metabolites, including 9-ci-retinoic acid, alpha-zearalenol, sphingosine, succinic acid, and L-dopa. Their expression was significantly negatively correlated with 23 metabolites, including (S)-2-methylate, linoleic acid, steric acid, aspartame, and yamogenin. Thirty-three genes, including *ncam1a*, *si:ch211-214p16.3*, *apoa1a*, *ugt1a7*, *slc13a2*, *cyp3a65*, *slc15a1b*, and *slc5a1* were significantly positively correlated with the expression of 23 metabolites, including (S)-2-methylate, linoleic acid, stearic acid, aspartame, yamogenin, and negatively correlated with the expression of 27 metabolites, including 9-ci-retinoic acid, alpha-zearalenol, sphingosine, succinic acid, and L-dopa (Figure 8FG).

The metabolic pathway involved in the differential expression of genes and metabolites between the Treatment B and model groups is that associated with ABC transporters (Supplementary Figure 6A). The main metabolites include xanthosine, L-homophenylalanine, phytosphingosine, L-dopa, (S)-2-methylmalate, prostaglandin E1, gingerol, porphybilinogen, and 16(R)-HETE, 8,9-DiHETrE. The main genes include *abcc5*, *fam133b*, *mt-co1*, *mt-co2*, *mt-nd1*, *mt-nd2*, *mt-atp6*, *krt4*. (Supplementary Figure 6B). Among these, three differentially expressed genes, i.e., *srsf5a*, *abcc5*, and *rbfox2* exhibited a significant positive correlation with 29 differential metabolites, including N2-m*alonyl-D-tryptophan, N-acetyl-L-phenylalanine, N-acetylaspartylglutamate, L-arginine, 3-indoleacrylate, N-acetylornithine, gamma-glutamylcysteine, and N6 acetyl-L-lysine. They exhibited a significant negative correlation with 21 differential metabolites, including xanthosine, sphingosine, 8,9-DiHETrE, (S)-2-methylmalate, succinic acid, and L-tyrosine. Forty-seven differentially expressed genes, including *cyt1*, *apoa1b*, *acta1b*, *mt-nd2*, *atp2a1*, *apoa2*, *apoa1a*, *apobb.1*, *mtnd3*, *tpt1*, *krt17*, *slc25a4*, were significantly negatively correlated and positively correlated with these 29 and 21 differentially expressed metabolites, respectively (Supplementary Figure 6CD).

The retinol metabolism pathway is the metabolic pathway in which Treatment C and the model group's differential metabolites and genes participate together(Supplementary Figure 7A). The main metabolites involved include 9-cis-retinoic acid, retinoyl b-glucuronide, and all-trans-retinoic acid; The main genes include *ugt1a7*, *bco1*, *cyp3a65*, *si:ch1073-13h15.3*, *cyp1a*, and *rdh5*. (Supplementary Figure 7B). Among these, the expression of 34 differentially expressed genes, including *atp1a1a.4*, *mbpa*, *zgc:136930*, *si:ch211-214p16.3*, *cdh17*, *mt-nd6*, *apobb.1*, *ugt1a7*, and *krt4* were significantly positively correlated with 32 differential metabolites, including isoxanthopterin, beta-alanyl-L-l-lysine, deoxyuridine, phytosphingosine, andrographide, 11,12-diHETrE, succinic acid, (S)-2-methylmalate, and xanthosine. The expression of these genes showed a significant negative correlation with 18 different metabolites, including allantoin, benzaldehyde, 3-Indoleacrylate, linoleic acid, erucic acid, N-acetyl-L-phenylalanine, and N-acetylornithine. Sixteen differentially expressed genes, including *hspa8*, *actc1b*, *rpl4*, *sf3b1*, *abcc5*, *srsf11*, and *cry1ba*, were significantly negatively and positively correlated with these 32 and 18 differentially expressed metabolites, respectively (Supplementary Figure 7CD).

5. Discussion

Hyperuricemia, as a metabolic disease, is caused by an imbalance in uric acid production and excretion and is closely related to hypertension, cardiovascular disease, chronic kidney disease, gout, and other conditions (Wang et al., 2018; Yanai et al., 2021). Research has shown that amino acid, carbohydrate, lipid, and energy metabolism are disrupted in patients with HUA and gout (Shen et al., 2021; Sui et al., 2023). In recent years, omics technology has developed rapidly, and metabolomics and transcriptomics have been widely applied for the diagnosis, treatment, and prediction of some diseases (Bujak et al., 2015; Lowe et al., 2017). *Gymnadenia Conopsea R.Br.*, as a traditional Chinese and Tibetan medicine, is widely used in the treatment of various diseases, such as lung deficiency, cough and asthma, chronic hepatitis, kidney deficiency, and neurasthenia (Morikawa et al., 2006; Zhang et al., 2020; Arzoo et al., 2021). Preliminary research showed that Gym significantly reduced the levels of uric acid, creatinine, and

urea nitrogen in zebrafish with HUA, and could regulate the activity of antioxidant enzymes [17]. This study is mainly based on the application of metabolomics and transcriptomics analysis to determine the metabolic mechanism of the ethanol extract derived from Gym on HUA zebrafish using PCA, PLS-DA, and (O) PLS-DA. The analysis was mainly based on the following three points: the metabolic pathways involved in the co-intervention of ethanol extracts of Gym and APL; the metabolic pathways involved in the production of differential metabolites involved in treatment derived from APL and Gym; and the metabolic pathways involved in the production of differential metabolites generated during the use of different extraction methods.

Compared with the control group, the levels of a total of 85 metabolites were found to have changed in the model group, including choline, 7-methyladenine, L-homophenylalanine, and 3-indoleacrylate, gamma glutamylalanine, 1-hexadecanol, palmitoleic acid, norepinephrine, prostaglandin A2 α-ketone acid, 5-aminovaleric acid, N-acetylornithine, guaninosuccinic acid, D-mannose, 4- (glutamylamine) butyric acid, inosine, N-acetylaspartate glutamate, 3'-adenosine, and 25 hydroxycholesterol; 41 other metabolites were upregulated. (S)2-methylmalic acid, 2,3-butanediol, citric acid, succinic acid, deoxycholic acid, deoxyuridine, EPA (d5), ε-(γ-L-pentenyl) - L-lysine, γ-glutamylcysteine, isoxanthopterin, L-arginine, L-aspartic acid, L-dopa, linoleic acid, L-canine uric acid, methyl jasmonate, methyl eugenol, nicotinamide ribose, plant sphingosine, prostaglandin I2, sphingosine, and 44 other metabolites were significantly downregulated. Compared with the model group, the APL and Gym group (Treatment A, B, and C groups) downregulated the levels of 6, 11, 12, and 9 of the above-mentioned metabolites, and upregulated the levels of 16, 15, 16, and 21 of the above-mentioned metabolites.

First, compared with the model group, the metabolic pathways influenced by different concentrations and doses of the ethanol extract of Gym and APL include those associated with PPAR signaling, arginine biosynthesis, arachidonic acid metabolism, linoleic acid metabolism, alanine, aspartate and glutamate metabolism, and ABC transport. The metabolites involved include linoleic acid, 13-L-peroxylinoleic acid, gamma-linolenic acid, 9-OxoODE, alpha-dimorphocolic acid, succinic acid, L-aspartic acid, citric acid, gamma-aminobutyric acid, prostaglandin H2, prostaglandin I2, 20-carboxy leukotriene B4, prostaglandin A2, 15-Deoxy-d-12, 8,9-DiHETrE, sphinganine, phytosphingosine, and all-trans-retinoic acid. The differentially expressed genes involved include *abcg2a*, *abcb11a*, *abca2*, *abcc2*, *abcc4*, *abca5*, *apoa1a*, *plin2*, *acsl5*, *cyp3a65*, *si: ch211-214p16.3*, *pck1*, *pck2*, *cd36*, etc. The treatment of HUA with Gym may be related to pathways associated with PPAR signaling, arginine biosynthesis, arachidonic acid metabolism, linoleic acid metabolism, alanine, aspartate and glutamate metabolism, ABC transport, and others.

Second, differential metabolites are involved in treatment with APL and Gym, and these differential metabolites and related genes are involved in metabolic pathways such as associated with mTOR signaling, D-arginine and D-ornithine metabolism, steroid hormone biosynthesis, sulfur metabolism, pentose and glucuronate interconversions, primary bile acid biosynthesis, purine metabolism, and propionate metabolism. These differential pathways may result in different therapeutic effects.

Finally, the differential metabolites generated with different extraction methods used with Gym are mainly those extracted with different ethanol concentrations. The main metabolic pathways involved in the generation of these differential metabolites and genes include those associated with alanine, aspartate, and glutamate metabolism, PPAR signaling, tyrosine metabolism, arginine biosynthesis, ABC transporters, retinol metabolism, linoleic acid metabolism, D-glutamine and D-glutamate metabolism, and oxidative phosphorylation. The differential metabolites involved in these differential pathways may lead to different therapeutic effects. Thus, the effective ingredient of Gym used in the treatment of HUA can be inferred.

In summary, the ethanol extract of Gym can exhibit therapeutic effects on HUA by participating in pathways associated with amino acid biosynthesis, amino acid metabolism, linoleic acid metabolism and ABC transport, unsaturated fatty acid biosynthesis, purine metabolism, PPRA signaling, etc.

6. Conclusion

The ethanol extract of Gym can exhibit therapeutic effects on HUA by participating in pathways associated with amino acid biosynthesis, amino acid metabolism, linoleic acid metabolism and ABC transport, unsaturated fatty acid biosynthesis, and PPRA signaling. This result provides a reference for identifying the metabolic mechanism by which Gym could be used for the treatment of HUA, and further exploration can be conducted from the perspectives of lipidomics and proteomics.

Abbreviations

Gym: *Gymnadenia conopsea (L.) R. Br.*; HUA: hyperuricemia; UHPLC-QE MS: ultra-high performance liquid chromatography-Q-Exactive mass spectrometry; SUA: serum uric acid; UA: uric acid; APL: allopurinol; XOD: xanthine oxidase; PO: potassium oxonate; XSS: xanthine sodium salt.

Declarations

Data availability statement

The original contributions presented in this study are included in the article/Supplementary material, further inquiries can be directed to the corresponding author.

Ethics statement

This animal study was reviewed and approved by the Center for Mitochondrial Health and Aging Research conducted by Yantai University (China). Recognize that the study was reported in accordance with ARRIVE guidelines.

Author contributions

TC: extraction process experiment, animal experiment, plotting and article writing. JL and FJ: literature compilation. CN and SY: literature search. YZ: funding acquisition and project advancement. All authors contributed to the article and approved the submitted version.

Funding sources

This research was funded by the Institute of Food Science and Technology, Xizang Academy of Agricultural and Animal Husbandry Sciences, grant number (Lhasa, China 850000); Natural Science Foundation of Xizang Autonomous Region (XZ202201ZR0015G); Xizang Finance Project (54000024210200019411); Major Science and Technology Project of Xizang Autonomous Region (XZ202201ZD0001N); Xizang Finance Project (XZNKYSPS-2024-C-045).

Acknowledgments

Thanks to the Center for Mitochondrial Health and Aging Research conducted by Yantai University (China) for providing the animal experiment platform; thanks to BioNovoGene (Suzhou, China), for helping with the metabolomics section; and the support of related projects in Xizang.

Conflict of interest

The authors declare that the research was conducted in the absence of any commercial or financial relationships that could be construed as a potential conflict of interest.

References

1. Abdelrazig, S., Safo, L., Rance, G. A., Fay, M. W., Theodosiou, E., Topham, P. D., Kim, D. H., Fernández-Castané, A, 2020. Metabolic characterisation of Magnetospirillum gryphiswaldense MSR-1 using LC-MS-based metabolite profiling. *RSC Adv*, 10(54), 32548-32560. https://doi.org/10.1039/d0ra05326k.
2. Abdulhafiz, F., Mohammed, A., Kayat, F., Bhaskar, M., Hamzah, Z., Podapati, S. K., Reddy, L. V, 2020. Xanthine Oxidase Inhibitory Activity, Chemical Composition, Antioxidant Properties and GC-MS Analysis of Keladi Candik (Alocasia longiloba Miq). *Molecules*, 25(11), 2658. https://doi.org/10.3390/molecules25112658.
3. Alexa A, Rahnenführer J, 2009. Gene set enrichment analysis with topGO. *Bioconductor Improv*. 27:1-26. http://www.mpi-sb.mpg.de/-alexa
4. Arzoo, S. H., Chattopadhyay, K., Parvin, T., Chattopadhyay, B, 2021. Amelioration of related complications by the combined usage of Gymnadenia orchidis Lindl and pumpkin seed in type 2 diabetic mice. *J Complement Integr Med*, 19(2), 345-352. https://doi.org/10.1515/jcim-2021-0499.
5. Bujak, R., Struck-Lewicka, W., Markuszewski, M. J., Kaliszan, R, 2015. Metabolomics for laboratory diagnostics. *J Pharm Biomed Anal,* 113, 108-120. https://doi.org/10.1016/j.jpba.2014.12.017.

6. Cai, M., Zhou, Y., Gesang, S., Bianba, C., Ding, L. S, 2006. Chemical fingerprint analysis of rhizomes of Gymnadenia conopsea by HPLC-DAD-MSn. *J Chromatogr B Analyt Technol Biomed Life Sci*, 844(2), 301-307. https://doi.org/10.1016/j.jchromb.2006.07.043.
7. Chen, L., Chu, C., Lu, J., Kong, X., Huang, T., Cai, Y. D, 2015. Gene Ontology and KEGG Pathway Enrichment Analysis of a Drug Target-Based Classification System. *PLoS One*, 10(5), e0126492. https://doi.org/10.1371/journal.pone.0126492.
8. Chen, T., Pubu, D., Zhang, W., Meng, S., Yu, C., Yin, X., Liu, J., Zhang, Y, 2022. Optimization of the extraction process and metabonomics analysis of uric acid-reducing active substances from Gymnadenia R.Br. and its protective effect on hyperuricemia zebrafish. *Front Nutr*, 9, 1054294. https://doi.org/10.3389/fnut.2022.1054294.
9. Gao, W., Sun, H. X., Xiao, H., Cui, G., Hillwig, M. L., Jackson, A., Wang, X., Shen, Y., Zhao, N., Zhang, L., Wang, X. J., Peters, R. J., Huang, L, 2014. Combining metabolomics and transcriptomics to characterize tanshinone biosynthesis in Salvia miltiorrhiza. *BMC Genomics*, 15, 73. https://doi.org/10.1186/1471-2164-15-73.
10. Gusev, A., Ko, A., Shi, H., Bhatia, G., Chung, W., Penninx, B. W., Jansen, R., de Geus, E. J., Boomsma, D. I., Wright, F. A., Sullivan, P. F., Nikkola, E., Alvarez, M., Civelek, M., Lusis, A. J., Lehtimäki, T., Raitoharju, E., Kähönen, M., Seppälä, I., Raitakari, O. T., Pasaniuc, B, 2016. Integrative approaches for large-scale transcriptome-wide association studies. *Nat Genet*, 48(3), 245-252. https://doi.org/10.1038/ng.3506.
11. Han, Y., Zhang, M., Lu, J., Zhang, L., Han, J., Zhao, F., Chen, H., Bao, Y., Jia, W, 2017. Hyperuricemia and overexcretion of uric acid increase the risk of simple renal cysts in type 2 diabetes. *Sci Rep*, 7(1), 3802. https://doi.org/10.1038/s41598-017-04036-6.
12. Horai, H., Arita, M., Kanaya, S., Nihei, Y., Ikeda, T., Suwa, K., Ojima, Y., Tanaka, K., Tanaka, S., Aoshima, K., Oda, Y., Kakazu, Y., Kusano, M., Tohge, T., Matsuda, F., Sawada, Y., Hirai, M. Y., Nakanishi, H., Ikeda, K., Akimoto, N., Nishioka, T, 2010. MassBank: a public repository for sharing mass spectral data for life sciences. *J Mass Spectrom*, 45(7), 703-714. https://doi.org/10.1002/jms.1777.
13. Huang, B., Hu, X., Wang, J., Li, P., Chen, J, 2019. Study on chemical constituents of herbal formula Er Miao Wan and GC-MS based metabolomics approach to evaluate its therapeutic effects on hyperuricemic rats. *J Chromatogr B Analyt Technol Biomed Life Sci*, 1118-1119, 101-108. https://doi.org/10.1016/j.jchromb.2019.04.032.
14. Huang, L., Deng, J., Chen, G., Zhou, M., Liang, J., Yan, B., Shu, J., Liang, Y., Huang, H, 2019. The anti-hyperuricemic effect of four astilbin stereoisomers in Smilax glabra on hyperuricemic mice. *J Ethnopharmacol*, 238, 111777. https://doi.org/10.1016/j.jep.2019.03.004.
15. Hui Xia, Huali Tang, Feng Wang, Xian Yang, Zhaodan Wang, Hechun Liu, Da Pan, Shaokang Wang, Guiju Sun, 2018. Metabolic effects of dietary supplementation of Lycium barbarum polysaccharides on serum and urine metabolomics in a young healthy male population. *Journal of Functional Foods*, 46: 440-448. https://doi.org/10.1016/j.jff.2018.04.060.

16. Hui, W., Yongliang, Y., Yongde, C., Guo, L., Li, L., Zhonglin, Y., Hui, J., Qinghua, H, 2016. Hypouricemic and Nephroprotective Effects of Emodinol in Oxonate-Induced Hyperuricemic Mice are Mediated by Organic Ion Transporters and OIT3. *Planta Med*, 82(4), 289–297. https://doi.org/10.1055/s-0035-1558212.
17. Jin, M., Yang, F., Yang, I., Yin, Y., Luo, J. J., Wang, H., Yang, X. F, 2012. Uric acid, hyperuricemia and vascular diseases. *Front Biosci (Landmark Ed)*, 17(2), 656–669. https://doi.org/10.2741/3950.
18. Kanehisa, M., Goto, S., 2000. KEGG: kyoto encyclopedia of genes and genomes. *Nucleic Acids Res*, 28(1), 27-30. https://doi.org/10.1093/nar/28.1.27.
19. Li, Y. J., Chen, L. R., Yang, Z. L., Wang, P., Jiang, F. F., Guo, Y., Qian, K., Yang, M., Yin, S. J., He, G. H, 2023. Comparative efficacy and safety of uricosuric agents in the treatment of gout or hyperuricemia: a systematic review and network meta-analysis. *Clin Rheumatol*, 42(1), 215-224. https://doi.org/10.1007/s10067-022-06356-z.
20. Lin, P. C., Wang, X., Zhong, X. J., Zhou, N., Wu, L., Li, J. J., Hu, Y. T., Shang, X. Y, 2021. Chemical characterization of a PD-1/PD-L1 inhibitory activity fraction of the ethanol extract from Gymnadenia conopsea. *J Asian Nat Prod Res*, 23(3), 235-249. https://doi.org/10.1080/10286020.2020.1844190.
21. Lowe, R., Shirley, N., Bleackley, M., Dolan, S., Shafee, T, 2017. Transcriptomics technologies. *PLoS Comput Biol*, 13(5), e1005457. https://doi.org/10.1371/journal.pcbi.1005457.
22. Marguerat, S., Bähler, J, 2010. RNA-seq: from technology to biology. *Cell Mol Life Sci*, 67(4), 569-579. https://doi.org/10.1007/s00018-009-0180-6.
23. Morikawa, T., Xie, H., Matsuda, H., Wang, T., Yoshikawa, M, 2006. Bioactive constituents from Chinese natural medicines. XVII. constituents with radical scavenging effect and new glucosyloxybenzyl 2-isobutylmalates from Gymnadenia conopsea. *Chem Pharm Bull (Tokyo)*, 54(4), 506-513. https://doi.org/10.1248/cpb.54.506.
24. Navarro-Reig, M., Jaumot, J., García-Reiriz, A., Tauler, R, 2015. Evaluation of changes induced in rice metabolome by Cd and Cu exposure using LC-MS with XCMS and MCR-ALS data analysis strategies. *Anal Bioanal Chem*, 407(29), 8835-8847. https://doi.org/10.1007/s00216-015-9042-2.
25. Oh, D. R., Kim, J. R., Choi, C. Y., Choi, C. H., Na, C. S., Kang, B. Y., Kim, S. J., Kim, Y. R, 2019. Effects of ChondroT on potassium Oxonate-induced Hyperuricemic mice: downregulation of xanthine oxidase and urate transporter 1. *BMC Complement Altern Med*, 19(1), 10. https://doi.org/10.1186/s12906-018-2415-2.
26. Rasmussen, J. A., Villumsen, K. R., Ernst, M., Hansen, M., Forberg, T., Gopalakrishnan, S., Gilbert, M. T. P., Bojesen, A. M., Kristiansen, K., Limborg, M. T, 2022. A multi-omics approach unravels metagenomic and metabolic alterations of a probiotic and synbiotic additive in rainbow trout (Oncorhynchus mykiss). *Microbiome*, 10(1), 21. https://doi.org/10.1186/s40168-021-01221-8.
27. Sapankaew, T., Thadanipon, K., Ruenroengbun, N., Chaiyakittisopon, K., Ingsathit, A., Numthavaj, P., Chaiyakunapruk, N., McKay, G., Attia, J., Thakkinstian, A, 2022. Efficacy and safety of urate-lowering agents in asymptomatic hyperuricemia: systematic review and network meta-analysis of

randomized controlled trials. *BMC Nephrol*, 23(1), 223. https://doi.org/10.1186/s12882-022-02850-3.

28. Shan, B., Chen, T., Huang, B., Liu, Y., Chen, J, 2021. Untargeted metabolomics reveal the therapeutic effects of Ermiao wan categorized formulas on rats with hyperuricemia. *Ethnopharmacol*, 281, 114545. https://doi.org/10.1016/j.jep.2021.114545.
29. Shang, X., Guo, X., Liu, Y., Pan, H., Miao, X., Zhang, J, 2017. Gymnadenia conopsea (L.) R. Br.: A Systemic Review of the Ethnobotany, Phytochemistry, and Pharmacology of an Important Asian Folk Medicine. *Front Pharmacol*, 8, 24. https://doi.org/10.3389/fphar.2017.00024.
30. Shen, X., Wang, C., Liang, N., Liu, Z., Li, X., Zhu, Z. J., Merriman, T. R., Dalbeth, N., Terkeltaub, R., Li, C., Yin, H. (2021). Serum Metabolomics Identifies Dysregulated Pathways and Potential Metabolic Biomarkers for Hyperuricemia and Gout. *Arthritis Rheumatol*, 73(9), 1738-1748. https://doi.org/10.1002/art.41733.
31. Sud, M., Fahy, E., Cotter, D., Brown, A., Dennis, E. A., Glass, C. K., Merrill, A. H., Jr, Murphy, R. C., Raetz, C. R., Russell, D. W., Subramaniam, S, 2007. LMSD: LIPID MAPS structure database. *Nucleic Acids Res*, D527-D532. https://doi.org/10.1093/nar/gkl838.
32. Sui, X., Xie, T., Xu, Y., Zhang, A., Zhang, Y., Gu, F., Li, L., Xu, Z., Chen, J, 2023. Protease-Activated Receptor-2 and Phospholipid Metabolism Analysis in Hyperuricemia-Induced Renal Injury. *Mediators Inflamm*, 2023, 5007488. https://doi.org/10.1155/2023/5007488.
33. Sun, Y. V., Hu, Y. J, 2016. Integrative Analysis of Multi-omics Data for Discovery and Functional Studies of Complex Human Diseases. *Adv Genet*, 93, 147-190. https://doi.org/10.1016/bs.adgen.2015.11.004.
34. Tan, Y., Wang, L., Gao, J., Ma, J., Yu, H., Zhang, Y., Wang, T., Han, L, 2021. Multiomics Integrative Analysis for Discovering the Potential Mechanism of Dioscin against Hyperuricemia Mice. J Proteome Res, 20(1), 645–660. https://doi.org/10.1021/acs.jproteome.0c00584.
35. Ujibe, K., Nishimura, K., Kashima, M., Hirata, H, 2021. Direct-TRI: High-throughput RNA-extracting Method for All Stages of Zebrafish Development. *Bio Protoc*, 11(17), e4136. https://doi.org/10.21769/BioProtoc.4136.
36. Wang, H., Zhang, H., Sun, L., Guo, W, 2018. Roles of hyperuricemia in metabolic syndrome and cardiac-kidney-vascular system diseases. *Am J Transl Res*, 10(9), 2749-2763. PMID: 30323864; PMCID: PMC6176241.
37. Wang, X., Zhong, X. J., Zhou, N., Cai, N., Xu, J. H., Wang, Q. B., Li, J. J., Liu, Q., Lin, P. C., Shang, X. Y., 2020. Rapid Characterizaiton of Chemical Constituents of the Tubers of Gymnadenia conopsea by UPLC-Orbitrap-MS/MS Analysis. *Molecules*, 25(4), 898. https://doi.org/10.3390/molecules25040898.
38. Want, E. J., Masson, P., Michopoulos, F., Wilson, I. D., Theodoridis, G., Plumb, R. S., Shockcor, J., Loftus, N., Holmes, E., Nicholson, J. K, 2013. Global metabolic profiling of animal and human tissues via UPLC-MS. *Nat Protoc*, 8(1), 17-32. https://doi.org/10.1038/nprot.2012.135.

39. Warren, C. R., O'Sullivan, J. F., Friesen, M., Becker, C. E., Zhang, X., Liu, P., Wakabayashi, Y., Morningstar, J. E., Shi, X., Choi, J., Xia, F., Peters, D. T., Florido, M. H. C., Tsankov, A. M., Duberow, E., Comisar, L., Shay, J., Jiang, X., Meissner, A., Musunuru, K., Cowan, C. A, 2017. Induced Pluripotent Stem Cell Differentiation Enables Functional Validation of GWAS Variants in Metabolic Disease. *Cell Stem Cell*, 20(4), 547-557.e7. https://doi.org/10.1016/j.stem.2017.01.010.
40. Wishart, D. S., Guo, A., Oler, E., Wang, F., Anjum, A., Peters, H., Dizon, R., Sayeeda, Z., Tian, S., Lee, B. L., Berjanskii, M., Mah, R., Yamamoto, M., Jovel, J., Torres-Calzada, C., Hiebert-Giesbrecht, M., Lui, V. W., Varshavi, D., Varshavi, D., Allen, D., Gautam, V, 2022. HMDB 5.0: the Human Metabolome Database for 2022. *Nucleic Acids Res*, 50(D1), D622-D631. https://doi.org/10.1093/nar/gkab1062.
41. Wu, J., Qiu, L., Cheng, X. Q., Xu, T., Wu, W., Zeng, X. J., Ye, Y. C., Guo, X. Z., Cheng, Q., Liu, Q., Liu, L., Xu, C. L., Zhu, G. J, 2017. Hyperuricemia and clustering of cardiovascular risk factors in the Chinese adult population. *Sci Rep*, 7(1), 5456. https://doi.org/10.1038/s41598-017-05751-w.
42. Wu, X., You, C, 2023. The biomarkers discovery of hyperuricemia and gout: proteomics and metabolomics. *PeerJ*, 11, e14554. https://doi.org/10.7717/peerj.14554.
43. Xia, J., Wishart, D. S, 2011. Web-based inference of biological patterns, functions and pathways from metabolomic data using MetaboAnalyst. *Nat Protoc*, 6(6), 743-760. https://doi.org/10.1038/nprot.2011.319.
44. Yanai, H., Adachi, H., Hakoshima, M., Katsuyama, H, 2021. Molecular Biological and Clinical Understanding of the Pathophysiology and Treatments of Hyperuricemia and Its Association with Metabolic Syndrome, Cardiovascular Diseases and Chronic Kidney Disease. *Int J Mol Sci*, 22(17), 9221. https://doi.org/10.3390/ijms22179221.
45. Yu, D., Fu, J., Wang, Y., Lu, F., Chen, P., Liu, S, 2023. Integrative metabolomics and network pharmacology to study the preventative impact of dioscin treatment on hyperuricemia. *Biomed Chromatogr*, 37(3), e5558. https://doi.org/10.1002/bmc.5558.
46. Yu, G, 2018. ClusterProfiler: an universal enrichment tool for functional and comparative study. *BioRxiv*, 256784. https://doi.org/10.1101/256784.
47. Zang, L., Shimada, Y., Nakayama, H., Kim, Y., Chu, D. C., Juneja, L. R., Kuroyanagi, J., Nishimura, N, 2019. RNA-seq Based Transcriptome Analysis of the Anti-Obesity Effect of Green Tea Extract Using Zebrafish Obesity Models. *Molecules*, 24(18), 3256. https://doi.org/10.3390/molecules24183256.
48. Zelena, E., Dunn, W. B., Broadhurst, D., Francis-McIntyre, S., Carroll, K. M., Begley, P., O'Hagan, S., Knowles, J. D., Halsall, A., HUSERMET Consortium, Wilson, I. D., Kell, D. B, 2009. Development of a robust and repeatable UPLC-MS method for the long-term metabolomic study of human serum. *Anal Chem*, 81(4), 1357-1364. https://doi.org/10.1021/ac8019366.
49. Zeng, J., Wang, J., Du, H., Zhao, X, 2007. Effect of Gymnadenia conopsea alcohol extract on pulmonary fibrosis of rats exposed to silica and the expression of tumor necrosis factor-alpha. *Journal of hygiene research*, 36(6), 674-678.
50. ZHANG Tian-e, CHEN Chao-yong, LI Shao-hua, CHEN Chong; LIU Weiwei; YAN Zhiyong, 2013. Effect of the extract of Gymnadenia conopsea on the blood lipid and liver function in ex-perimental

hyperlipidemia rats. *Lishizhen Medicine and Material Medica Research*, 24(04): 865-867.

51. Zhang, S., Wang, Y., Cheng, J., Huangfu, N., Zhao, R., Xu, Z., Zhang, F., Zheng, W., Zhang, D, 2019. Hyperuricemia and Cardiovascular Disease. *Curr Pharm Des*, 25(6), 700-709. https://doi.org/10.2174/1381612825666190408122557
52. Zhang, Y., Li, Q., Wang, F., Xing, C, 2019. A zebrafish (danio rerio) model for high-throughput screening food and drugs with uric acid-lowering activity. *Biochem Biophys Res Commun*, 508(2), 494-498. https://doi.org/10.1016/j.bbrc.2018.11.050.
53. Zhang, Y., Liu, L., Liang, C., Zhou, L., Tan, L., Zong, Y., Wu, L., Liu, T, 2020. Expression Profiles of Long Noncoding RNAs in Mice with High-Altitude Hypoxia-Induced Brain Injury Treated with Gymnadenia conopsea (L.) R. Br. *Neuropsychiatr Dis Treat*, 16, 1239-1248. https://doi.org/10.2147/NDT.S246504.
54. Zhang, Y., Zhang, H., Chang, D., Guo, F., Pan, H., Yang, Y, 2018. Metabolomics approach by 1H NMR spectroscopy of serum reveals progression axes for asymptomatic hyperuricemia and gout. *Arthritis Res Ther*, 20(1), 111. https://doi.org/10.1186/s13075-018-1600-5.
55. Zhou J ,Wang Z ,Zhang Z, 2024. Modulation of gut microbiota and serum metabolome by Apostichopus japonicus derived oligopeptide in high-fructose diet-induced hyperuricemia in mice. *Food Science and Human Wellness*, 1-21.doi:10.1750.TS.20240227.1622.040.

Figures

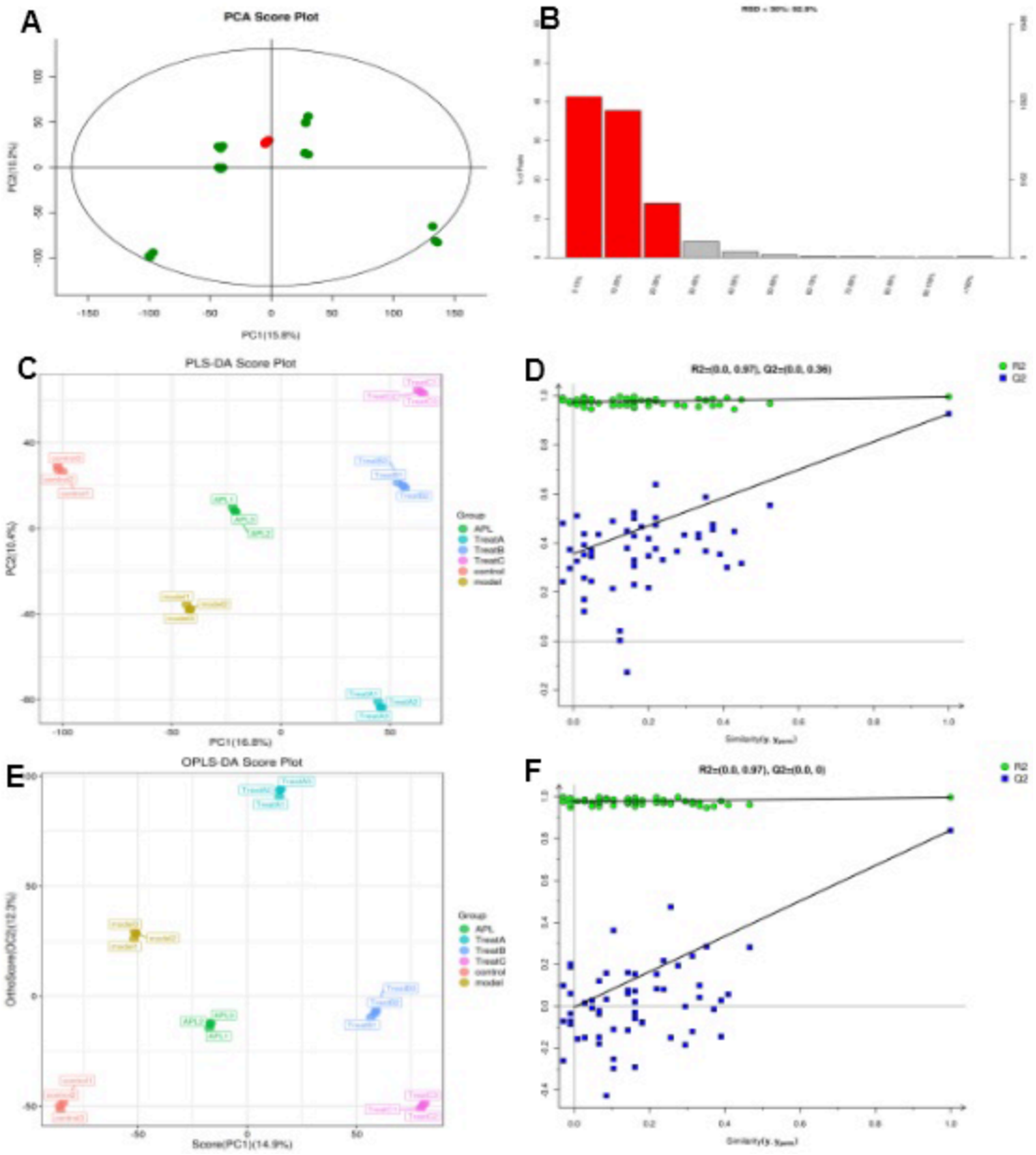


Figure 1

Multivariate statistical analysis chart. (A): The PCA score chart of samples; (B): RSD distribution map; (C)&(E): PLS-DA and OPLS-DA score maps of samples; (D)&(F): Replacement test results of PLS-DA and OPLS-DA samples.

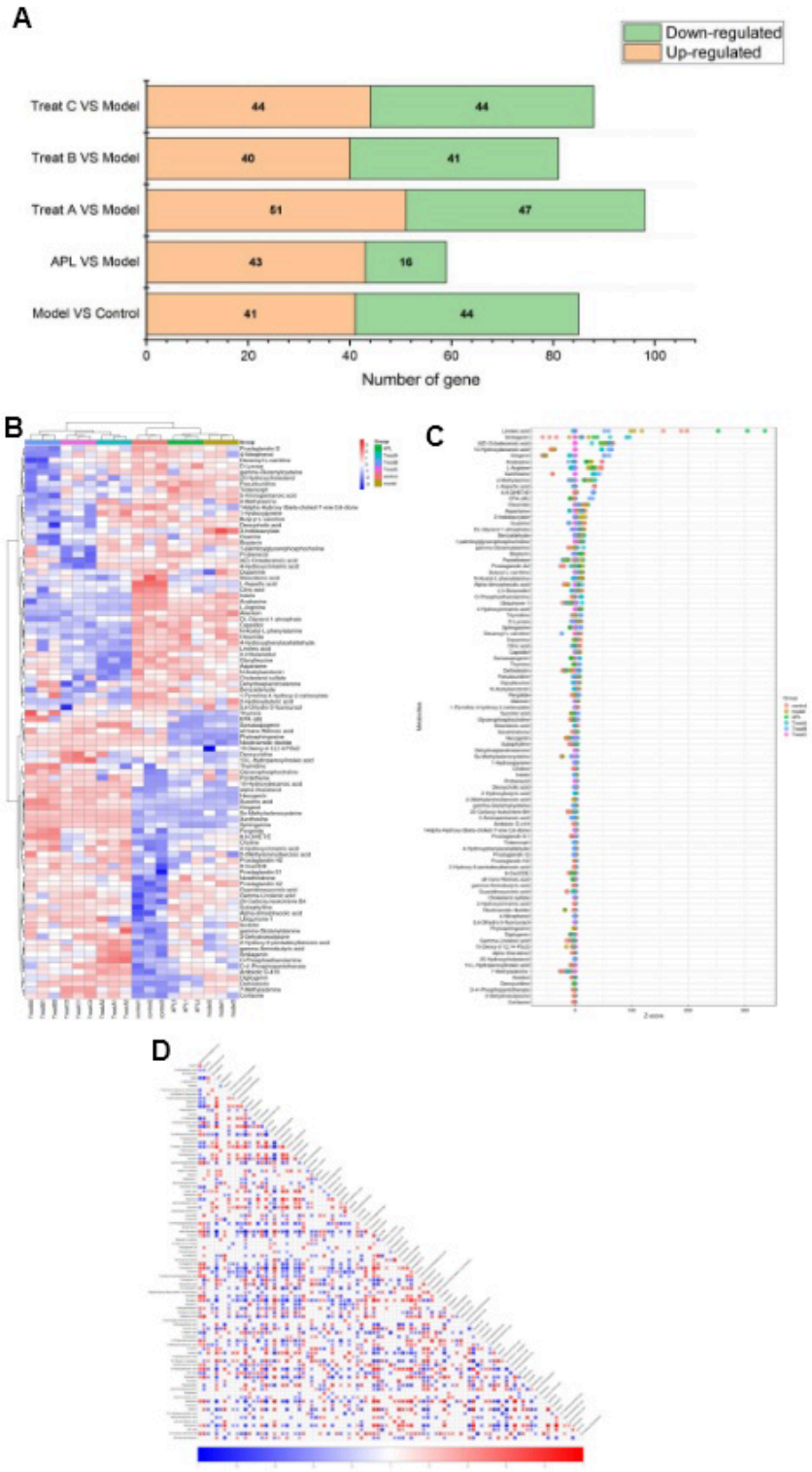


Figure 2

(A) Statistical chart of differential metabolites in different comparison groups; (B) The heat map of differential metabolites;(C) The Z-score plot of differential metabolites; (D) The correlation chart of differential metabolites.

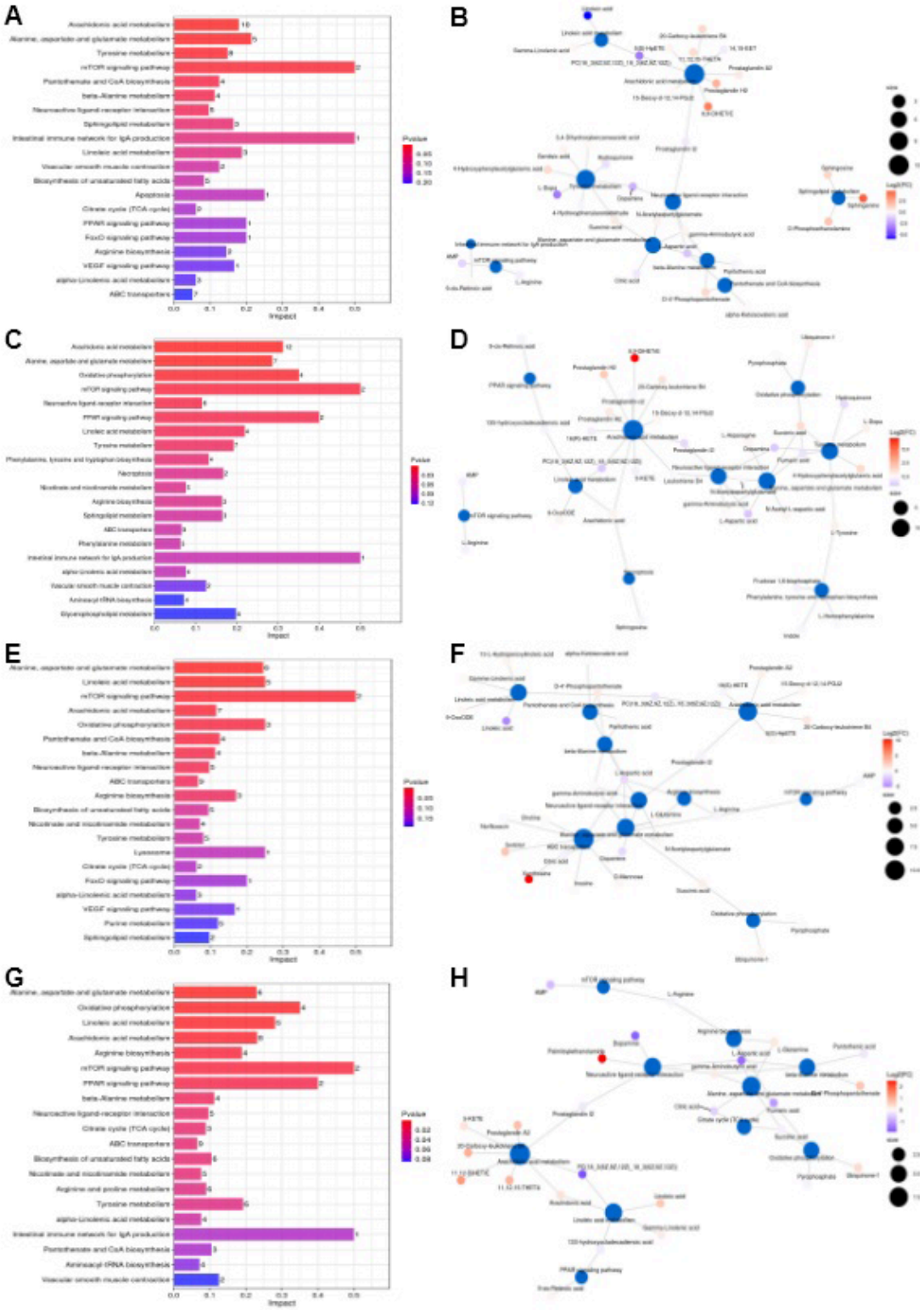


Figure 3

KEGG enrichment analysis, enrichment bar graph and network graph. (A) & (B) : Treatment A vs Control; (C) & (D) : Treatment B VS Control; (E) & (F): Treatment C VS Control; (G) & (H) : APL VS Control.

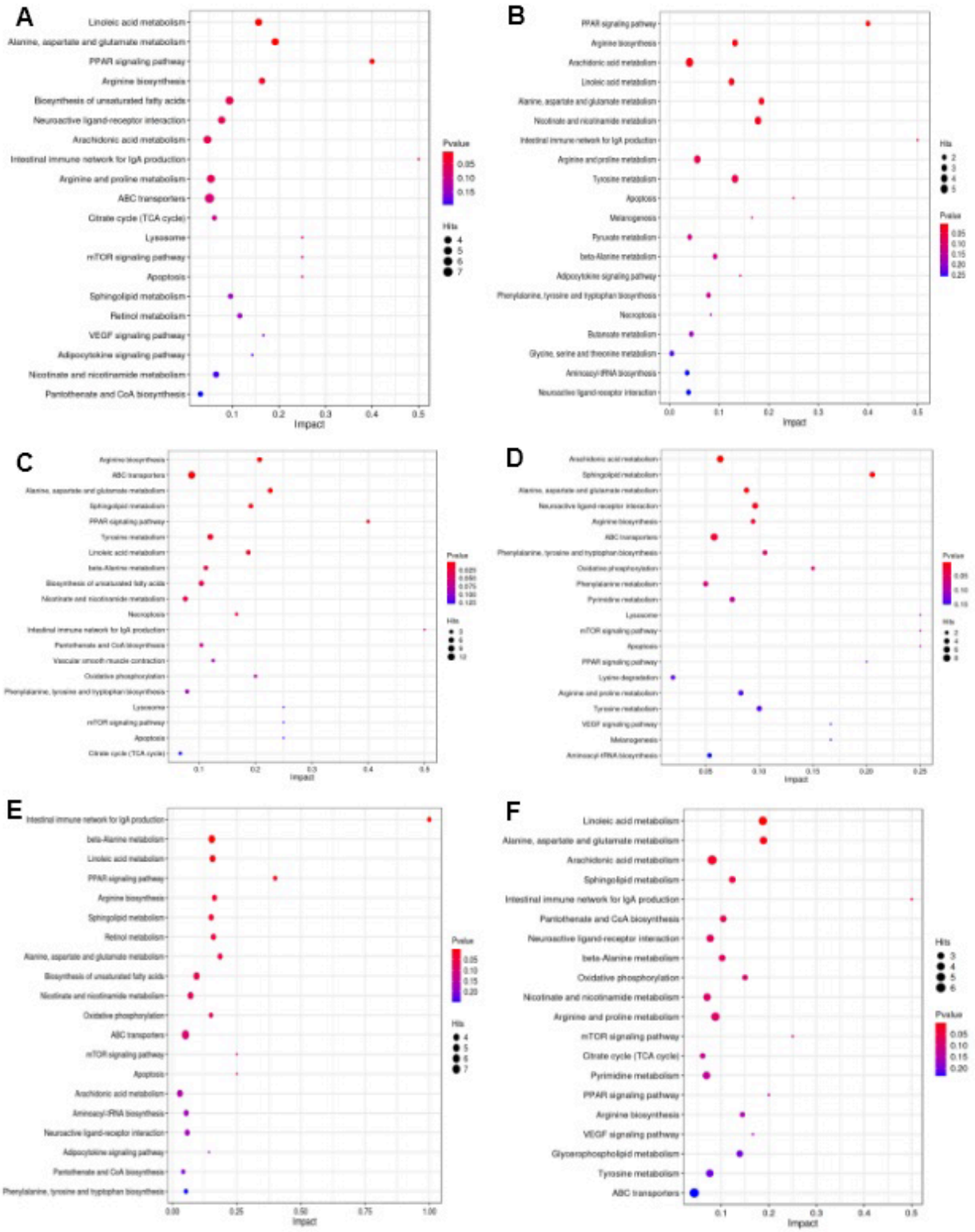


Figure 4

KEGG metabolic pathway analysis (A) : Control vs. Model; (B) : APL VS Model; (C) : Treatment A VS Model; (D) : Treatment B VS Model; (E) : Treatment C VS Model; (F) Overall metabolite pathway visualization (top 20).

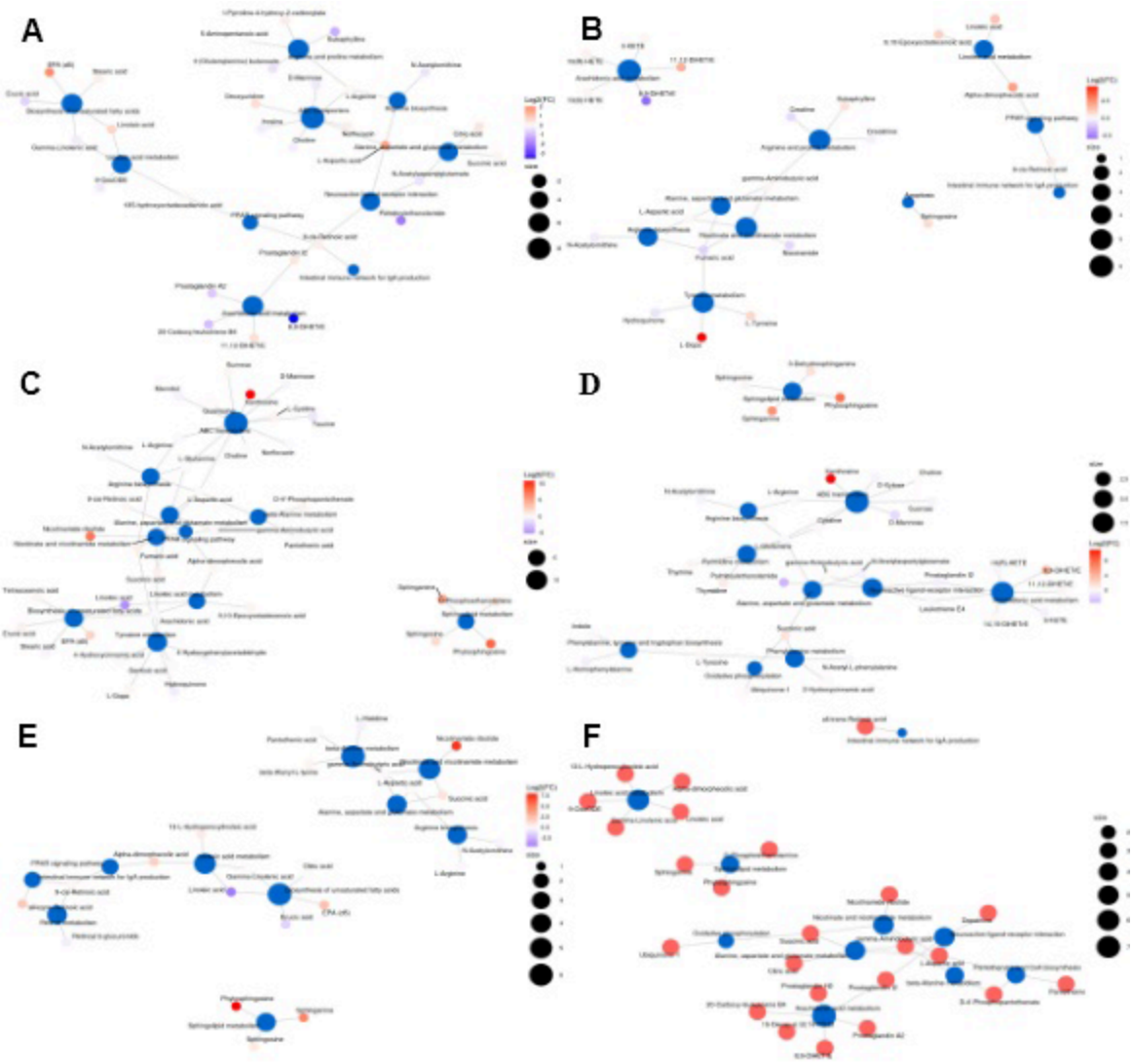


Figure 5

KEGG metabolic network analysis (A) : Control vs. Model; (B) : APL VS Model; (C) : Treatment A VS Model; (D) : Treatment B VS Model; (E) : Treatment C VS Model; (F)All groups.

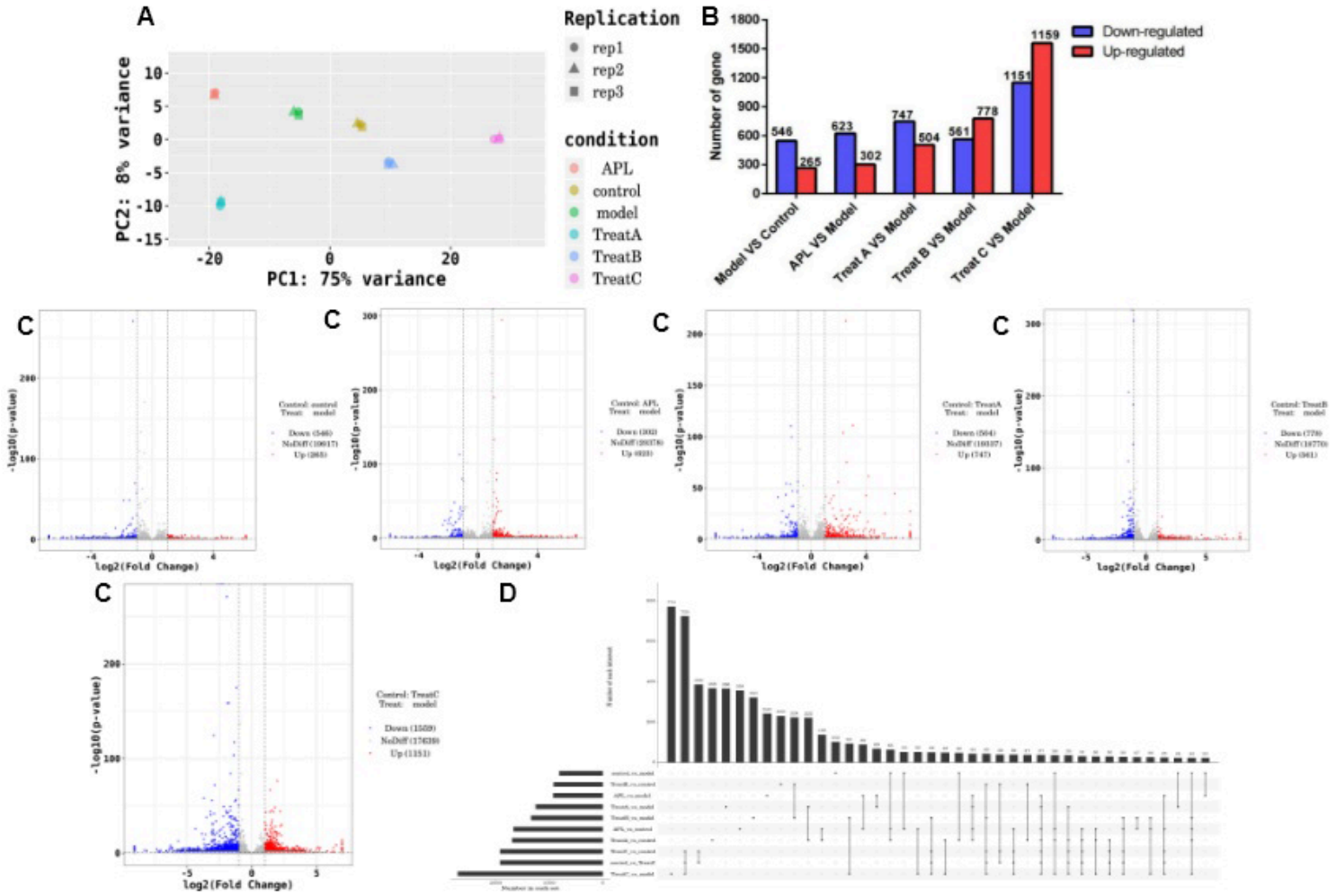


Figure 6

Transcriptomic analysis (A) PCA analysis chart; (B) Statistical analysis of differentially expressed genes among different comparison groups; (C1-C5): Volcano plot of differentially expressed genes in different comparison groups; (D) Statistical Upset plot of differential expression analysis results

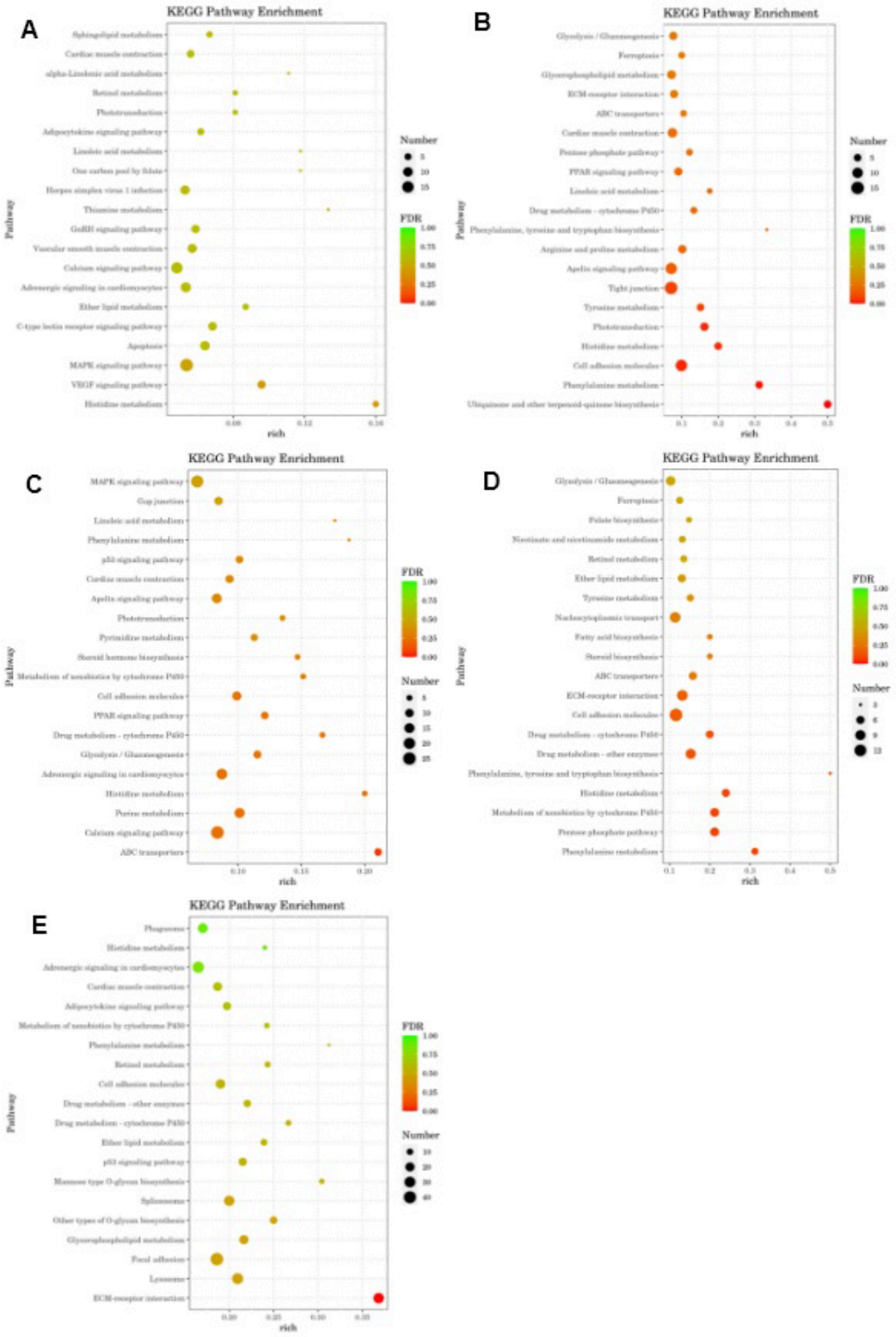


Figure 7

KEGG enrichment analysis of differentially expressed genes. (A): Control VS Model; (B): APL VS Model; (C): Treatment A VS Model; (D): Treatment B VS Model; (E): Treatment C VS Model.

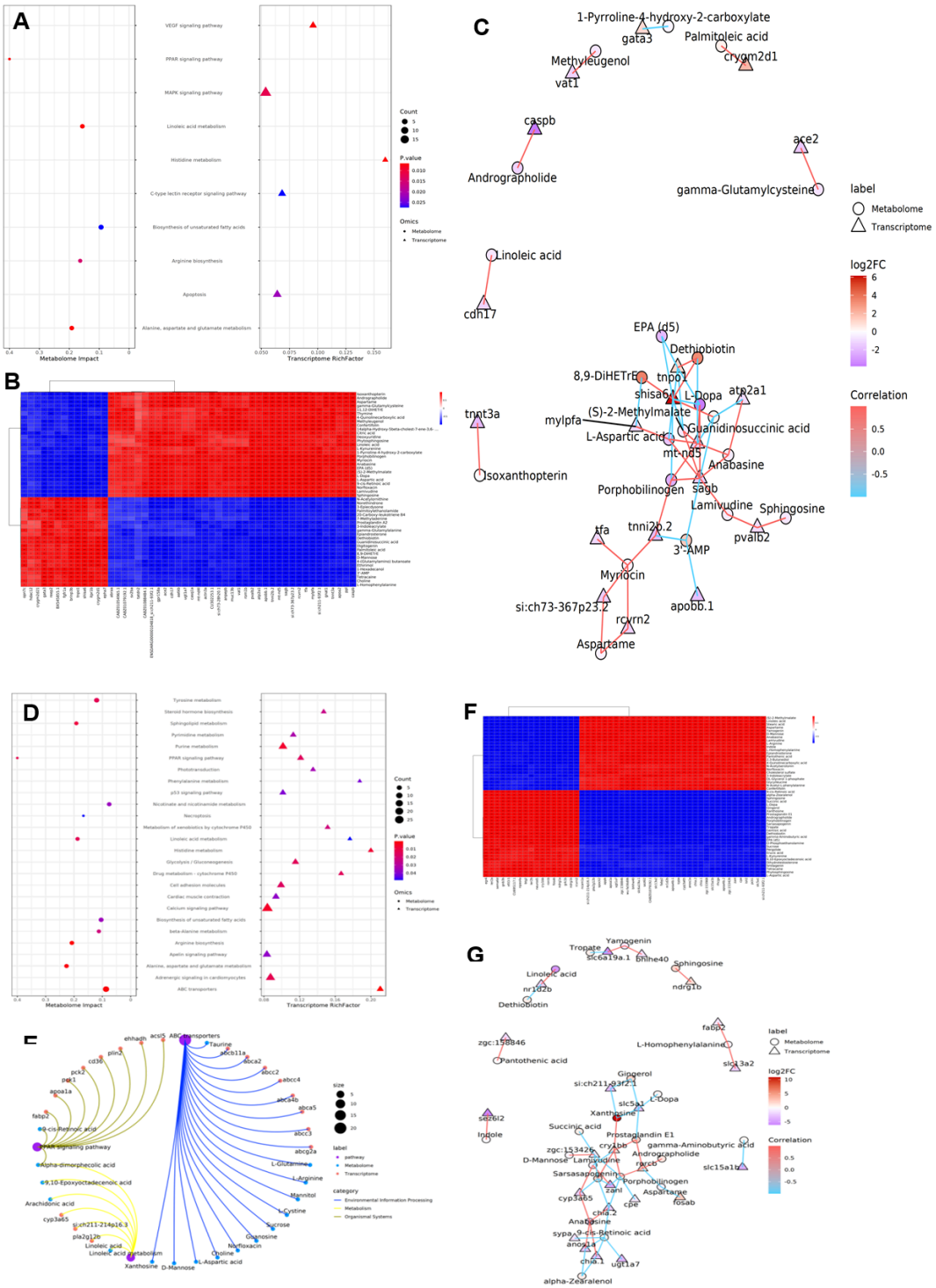


Figure 8

Analysis of the correlation between Model VS Control (A-C) and Treatment A VS Model (D-G). (A-C) KEGG enrichment network diagram, Associated heat map, Correlation network diagram of Model VS Control; (D-G) KEGG enrichment network diagram, KEGG enrichment network diagram, Associated heat map, Correlation network diagram of Treatment A VS Model.

Supplementary Files

This is a list of supplementary files associated with this preprint. Click to download.

- Supplementarymaterials.zip